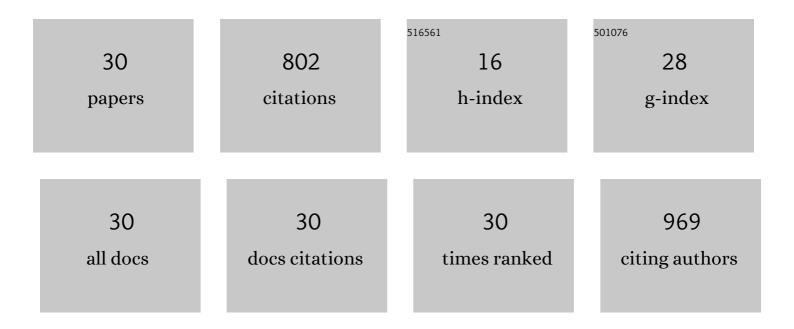
Puspendu Sahu

List of Publications by Year in descending order

Source: https://exaly.com/author-pdf/7178711/publications.pdf Version: 2024-02-01



DUCDENDU SAHU

#	Article	IF	CITATIONS
1	Newer insights into the discrimination of pole mechanisms of twinning in a face-centered cubic high-Mn steel. Materialia, 2022, 21, 101349.	1.3	3
2	Dislocation substructures in tensile deformed Fe–Mn–Al–C steel. Materials Letters, 2021, 282, 128691.	1.3	4
3	X-ray line profile analysis of the deformation microstructure in a medium-grained Fe-Mn-Al-C austenitic steel. Materials Characterization, 2021, 172, 110833.	1.9	9
4	On the mechanism of cross-slip induced dislocation substructure formation in an high-Mn steel. Materialia, 2021, 15, 101042.	1.3	12
5	A quantitative assessment on the contribution of various dislocation substructures to flow stress in a fine-grain high-Mn steel. Materials Letters, 2021, 300, 130216.	1.3	1
6	Phase changing stearate ions as active fillers in multifunctional carboxylated acrylonitrile–butadiene composite: Exploring the role of zinc stearate. Journal of Applied Polymer Science, 2020, 137, 48271.	1.3	11
7	Simultaneous twinning nucleation mechanisms in an Fe–Mn–Si–Al twinning induced plasticity steel. Acta Materialia, 2017, 132, 264-275.	3.8	28
8	The effect of the order-disorder transition on the electrical, magnetic and mechanical properties of Vicalloy I. Intermetallics, 2017, 81, 73-79.	1.8	6
9	Correlation of Microstructure and Texture in a Two-Phase High-Mn Twinning-Induced Plasticity Steel During Cold Rolling. Metallurgical and Materials Transactions A: Physical Metallurgy and Materials Science, 2017, 48, 4842-4856.	1.1	8
10	Electron microscopy study on grain boundary characterizations of Fe–Co–V alloy during annealing. Vacuum, 2015, 114, 1-5.	1.6	8
11	An effective stacking fault energy viewpoint on the formation of extended defects and their contribution to strain hardening in a Fe–Mn–Si–Al twinning-induced plasticity steel. Acta Materialia, 2015, 86, 69-79.	3.8	87
12	Enhancement of mechanical properties of a TRIP-aided austenitic stainless steel by controlled reversion annealing. Materials Science & Engineering A: Structural Materials: Properties, Microstructure and Processing, 2015, 628, 154-159.	2.6	49
13	Indentation property and corrosion resistance of electroless nickel–phosphorus coatings deposited on austenitic high-Mn TWIP steel. Applied Surface Science, 2015, 356, 1-8.	3.1	34
14	Micro-structure, optical properties and ac conductivity of rare earth double perovskite oxides: Sr2ErNbO6. Physica B: Condensed Matter, 2013, 422, 78-82.	1.3	10
15	Studies on Martensite Transformation in a Metastable Austenitic Cr-Mn Stainless Steel. Materials Science Forum, 2013, 762, 424-430.	0.3	3
16	Effects of Carbon Content and Cooling Path on the Microstructure and Properties of TRIP-aided Ultra-High Strength Steels. ISIJ International, 2013, 53, 337-346.	0.6	15
17	Structural and microstructural evolution due to increasing Co substitution in Ni1â^xCoxFe2O4: An X-ray diffraction study using the Rietveld method. Materials Chemistry and Physics, 2011, 128, 365-370.	2.0	16
18	Stability of austenite and quasi-adiabatic heating during high-strain-rate deformation of twinning-induced plasticity steels. Scripta Materialia, 2010, 62, 5-8.	2.6	28

Puspendu Sahu

#	Article	IF	CITATIONS
19	Shape- and field-dependent Morin transitions in structured α-Fe2O3. Journal of Magnetism and Magnetic Materials, 2009, 321, 2925-2931.	1.0	62
20	Microstructure characterization of mechanosynthesized nanocrystalline NiFe2O4 by Rietveld's analysis. Physica E: Low-Dimensional Systems and Nanostructures, 2007, 39, 175-184.	1.3	55
21	Structure and microstructure evolution during martensitic transformation in wrought Fe–26Mn–0.14C austenitic steel: an effect of cooling rate. Journal of Applied Crystallography, 2007, 40, 354-361.	1.9	19
22	Lattice imperfections in intermetallic Ti–Al alloys: an X-ray diffraction study of the microstructure by the Rietveld method. Intermetallics, 2006, 14, 180-188.	1.8	21
23	Internal friction study on fcc/hcp martensitic transformations in thermomechanically treated Fe–28Mn–6Si–5Cr–0.53Nb–0.06C (mass%) alloys. Materials Science & Engineering A: Structural Materials: Properties, Microstructure and Processing, 2006, 442, 404-408.	2.6	10
24	Vibration mitigation by the reversible fcc/hcp martensitic transformation during cyclic tension–compression loading of an Fe–Mn–Si-based shape memory alloy. Scripta Materialia, 2006, 54, 1885-1890.	2.6	91
25	Bainite and stress-induced martensite in an AISI type 300 steel: an X-ray diffraction study of the microstructure by the Rietveld method. Journal of Applied Crystallography, 2005, 38, 112-120.	1.9	16
26	X-ray diffraction studies of the decomposition and microstructural characterization of cold-worked powders of Cu–15Ni–Sn alloys by Rietveld analysis. Journal of Alloys and Compounds, 2004, 377, 103-116.	2.8	40
27	Microstructural characterization of the evoluted phases of ball-milled α-Fe2O3 powder in air and oxygen atmosphere by Rietveld analysis. Materials Chemistry and Physics, 2003, 82, 864-876.	2.0	18
28	Microstructure characterization of polymorphic transformed ball-milled anatase TiO2 by Rietveld method. Materials Chemistry and Physics, 2003, 77, 153-164.	2.0	67
29	Microstructural characterization of stress-induced martensites evolved at low temperature in deformed powders of Fe–Mn–C alloys by the Rietveld method. Journal of Alloys and Compounds, 2002, 346, 158-169.	2.8	38
30	Microstructural characterization of Fe–Mn–C martensites athermally transformed at low temperature by Rietveld method. Materials Science & Engineering A: Structural Materials: Properties, Microstructure and Processing, 2002, 333, 10-23.	2.6	33